COMPDYN 2013
4th ECCOMAS Thematic Conference on
Computational Methods in Structural Dynamics and Earthquake Engineering
M. Papadrakakis, V. Papadopoulos, V. Plevris (eds.)
Kos Island, Greece, 12–14 June 2013

# A MULTI-DIRECTIONAL ABSORBING LAYERS FOR SEISMIC WAVE PROPAGATION IN UNBOUNDED DOMAIN BY USING HETEROGENEOUS MULTI-TIME STEP SUB-DOMAIN METHODS

**Zafati E.**[1], **Brun M.**[1], **and Irini DJ.M.**[1]

[1]INSA de Lyon
Batiment Coulomb 20, Avenue A. Einstein 69621 Villeurbanne cedex (France)
e-mail: eliass.zafati@insa-lyon.fr

**Keywords:** wave propagation, Rayleigh damping, sub domains, code coupling.

**Abstract.** *It is well known that the elastic wave propagation predicted by the FEM suffers from the difficulty to correctly reproduce the unbounded media: spurious waves are reflected at the FEM model at the artificial boundaries. Variant techniques may be introduced to reduce the spurious reflections at the boundaries, such as the infinite elements, the absorbing boundary conditions or the perfect matched layers. Nonetheless, the most efficient strategy, such as the perfect matched layer, leads to an important implementation effort in existing FE softwares. Recently, a simplified approach proposed by Semblat et al. (2010) consists in introducing classical Rayleigh formulation in a layer subdomain, surrounding the domain under investigation; the purpose of this artificial layer is to damp the incident seismic waves while minimizing the spurious reflected waves towards the studied domain. The objective of this work is to enhance this methodology by taking advantage of the subdomain methods. The GC method, proposed ten years ago by Combescure and Gravouil, enables to decompose a finite element mesh into several partitions and to use in each partition the suitable time integrator with its own time step. Therefore, the coupling method is heterogeneous, allowing to couple different time integrators and multi-time steps in the sense that very different time steps depending on the subdomains can be adopted. An external coupling software, based on the GC method, are developed to enable multi-time step explicit/implicit co-computations. It makes to interact in time an explicit FE code (Europlexus), associated with fine time step for the domain of interest, with an implicit FE code (Cast3m) handling the absorbing boundary layers by using a Rayleigh viscous damping matrix. Large time steps can be adopted for the absorbing boundary layers. The reduction of the spurious wave reflections at the interface has been optimized as well as the ability of the absorbing layers to damp the transmitted waves. The relevance and the numerical efficiency of the multi-time step implicit absorbing boundary layer strategy are compared with classical absorbing boundary conditions.*

## 1 Introduction

The simulation of the soil interaction problems [1] using the Finite Element method requires the modeling of an unbounded medium. Efficient numerical methods have to be set up, minimizing the number of operations while maintaining the accuracy of computation. For modeling the wave propagation in soils, we need a very huge mesh to avoid the artificial reflected waves at the boundaries of the domain of interest. However, such model becomes more costly in computation time, especially when we work with complex structures. To reduce the FE model for the domain of interest, several methods have been developed which consist in adding artificial conditions at the boundaries such as the PML (Perfect Matched Layers) [2], absorbing boundaries [3] or infinite elements [4]. The aim of these techniques is to absorb the energy coming from the field of interest without generating important spurious waves.

One technique for absorbing the incident waves is to introduce artificial layers at the boundaries. This method has been used in some problems by introducing the Rayleigh matrix [5] in elastic layers. The Rayleigh matrix is simply expressed as a linear combination of the mass matrix and the stiffness matrix. This method turns out to be efficient and easy to implement. However, the amount of spurious waves reflected at the boundaries is not easy to be predicted as well as the optimal thickness for minimizing the reflected waves while optimizing the damping in the Rayleigh medium.

The Rayleigh matrix has been generalized following the work of Caughey [6]. The use of the Rayleigh matrix for soil dynamics problems is not obvious because the behavior of the derived Rayleigh material can be viewed as unphysical. However, Semblat $et\ al.$ gives a rheological interpretation of this material and shows the similarity between this material and the Maxwell material [7].

As already mentioned, the optimization of the computation time is an important criterion to work with complex geometry problems. Subdomain methods with multi time steps depending on the subdomains can be good candidates for reducing the computation time. Gravouil and Combescure [8] proposed an efficient partitioning method, denoted as GC method, able to couple several time integration schemes from the Newmark family with different time steps. The method follows a dual Schur approach by ensuring the velocity continuity at the interface through Lagrange multipliers. The method is proved to be stable using the so-called energy method [9]. . It leads to the first order of accuracy when coupling second order accuracy time integration schemes due to a slight spurious dissipation at the interface as soon as different time steps are adopted. Implicit/Explicit multi-time step co-computations, using a coupling software based on the GC method, have been validated in comparison to full explicit computation for reinforced concrete structures subjected to earthquake loading [10].

In the present paper we suggest to:

1 - show the link between the Rayleigh damping and the Kelvin-Voigt viscoelastic material. We seek to obtain a strong from for wave propagation in the Rayleigh medium in order to determine the optimal conditions for minimizing the reflected waves between a non dissipative medium with a Rayleigh medium. These conditions will be determined for harmonic waves.

2 - Validate the previous optimal conditions at the interface by considering numerical examples: first without subdomain decomposition for a 1D wave propagation problem and second with the GC coupling method for the 2D Lamb's problem [11]. In this latter, two different Finite Element codes will be used into an Explicit/Implicit multi time step co-computation: Europlexus [12] based on the explicit scheme and Cast3m [13] based onthe implicit scheme.

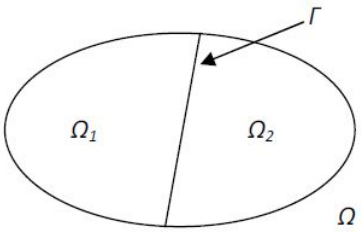


Figure 1: Domain $\Omega$ divided into two subdomains $\Omega_1$and$\Omega_2$

## 2 Rayleigh damping

In this part, it is proposed to study a problem in a continuum medium divided into two subdomains separated by the interface denoted as $\Gamma$: the subdomain $\Omega_1$ with a linear elastic behavior and the subdomain $\Omega_2$ with a damping behavior defined later. A strong form for the wave propagation in the damped subdomain is proposed. It will be shown that the discretized form of the damped subdomain exactly corresponds to the introduction of the Rayleigh matrix into the classical discretized in space equation of motion. Once obtained the strong form for the wave propagation in the Rayleigh damping medium, the interface problem can be analytically studied, by writing for harmonic waves the continuity of displacements and the stress equilibrium at the interface.

Linear elastic behavior is assumed, with an infinitesimal strain tensor defined by:

$$\epsilon(u) = \frac{1}{2}(\nabla u + \nabla^t u) \tag{1}$$

$u$ being the field displacement vector.

### 2.1 The boundary value problem (strong form)

Let $\Omega$ a bounded open set from $\mathbb{R}^3$ with a regular boundary. We assume that the domain is divided into two parts $\Omega_1$ and $\Omega_2$ illustrated in Figure 1 such as : $\Omega_1 \cap \Omega_2 = \varnothing$ and $\partial\Omega_1 \cap \partial\Omega_2 = \Gamma$.

**Subdomain $\Omega_1$ :**

It is assumed that the medium $\Omega_1$ is elastic linear characterized by the density $\rho_1$ and the Lame coefficients $\lambda_1$ and $\mu_1$. We call $E_1$,$\nu_1$ the Young's modulus and the Poisson's coefficient of this material. The displacement vector field $u_1$ is governed by the following equations:

$$\rho_1 \partial_t^2 u_1 = div(\sigma_1(u_1)) \tag{2}$$

$$\sigma_1 = \lambda_1 tr(\epsilon(u_1)) + 2\mu_1 \epsilon(u_1) \tag{3}$$

with the boundary conditions:

$$\sigma_1.n_1 = g_{1n} \ \ on \ \ \ \partial\Omega_{1n} \tag{4}$$

$$u_1 = u_{1d} \ \ on \ \ \partial\Omega_{1d} \tag{5}$$

Here $\partial\Omega_{1d}$ and $\partial\Omega_{1n}$ are subsets of the boundary with $\partial\Omega_{1n} \cup \partial\Omega_{1d} = \partial\Omega_1 \setminus \Gamma$ and $\partial\Omega_{1n} \cap \partial\Omega_{1d} = \varnothing$.

The initial conditions are:

$$u_1(x \in \Omega_1, t = 0) = 0 \tag{6}$$

$$\partial_t u_1(x \in \Omega_1, t = 0) = 0 \tag{7}$$

**Subdomain $\Omega_2$:**

We assume that the displacement vector field $u_2$ is governed by the following equations:

$$\rho_2 \, \partial_t^2 u_2 + a \, \rho_2 \, \partial_t u_2 = div(\sigma_2(u_2)) \tag{8}$$

$$\sigma_2 = \lambda_2 \, tr(\epsilon(u_2)) + 2\mu_2 \epsilon(u_2) + b \, (\lambda_2 \, tr(\epsilon(\partial_t u_2)) + 2\mu_2 \, \epsilon(\partial_t u_2)) \tag{9}$$

with $a,\ b,\ \lambda_2,\ \mu_2$ being positive integers.

It is clear from the Eq. (9) that the material has the behavior of a Kelvin-Voigt viscoelastic material, with $b$ corresponding to the characteristic time parameter. From Eq. (8), it can be seen that a dashpot, characterized by the damping coefficient $a\,\rho_2$, has been added as classically done for a damped oscillator. The parameters $\lambda_2, \mu_2$ are called the Lame coefficients. Similarly, $E_2$ and $\nu_2$ are the Young's modulus and the Poisson's ratio of the Kelvin-Voigt viscoelastic material.

Particular boundary conditions are given as follows:

$$\sigma_2.n_2 = 0 \; on \quad \partial\Omega_{2n} \qquad\qquad u_2 = 0 \; on \;\; \partial\Omega_{2d} \tag{10}$$

with

$$\partial\Omega_{2n} \cup \partial\Omega_{2d} = \partial\Omega_2 \setminus \Gamma \qquad\qquad \partial\Omega_{2n} \cap \partial\Omega_{2d} = \varnothing \tag{11}$$

The initial conditions are taken as:

$$u_2(x \in \Omega_2, t = 0) = 0 \qquad\qquad \partial_t u_2(x \in \Omega_2, t = 0) = 0 \tag{12}$$

**The interface :**

Figure 2 illustrates the conventional orientations of the normal vectors. The continuity of displacements and equilibrium of stresses are given by :

$$\sigma_2.n_2 = -\sigma_1.n_1 \quad on \quad \Gamma \qquad\qquad u_1 = u_2 \quad on \quad \Gamma \tag{13}$$

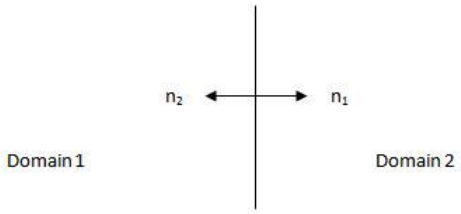


Figure 2: the normal vectors at the interface

### 2.2 The problem discretized in space

We assume that the problem presented above is well-posed ([16]). Through the weak formulation and the finite element approximation, it can be proved that the problem in the dicretized space is given by:

$$M_1\ddot{U}_1 + K_1U_1 + L_1^T\hat{\lambda} = F_1^{ext} \tag{14}$$

$$M_2\ddot{U}_2 + K_2U_2 + (a\ M_2 + b\ K_2)\dot{U}_2 + L_2^T\hat{\lambda} = 0 \tag{15}$$

$$L_1U_1 + L_2U_2 = 0 \tag{16}$$

Here $U_1$ and $U_2$ are the displacements vectors in the discretized space, $M_i$ and $K_i$ are the mass and the stiffness matrices related to the subdomain $i$, $i = \{1, 2\}$. The vector $\hat{\lambda}$ can be interpreted as the nodal forces at the interface. The operators $L_1$ and $L_2$ are defined as Boolean matrices which select the nodes belonging to the interface.

The Dirichlet and the Neumann conditions are given by:

$$U_1 = U_{1d}\ on\ \partial\Omega_{1d} \qquad\qquad U_2 = 0\ on\ \partial\Omega_{2d} \tag{17}$$

$$U_1(t=0) = \dot{U}_1(t=0) = 0\ on\ \Omega_1 \tag{18}$$

$$U_2(t=0) = \dot{U}_2(t=0) = 0\ on\ \Omega_2 \tag{19}$$

It can be observed that the term $a\ M_2 + b\ K_2$ appears in the Eq. (15) which corresponds to the Rayleigh matrix. Thus, it can be shown that the proposed strong from given in Eqs. (8) (9) corresponds to the introduction of the classical Rayleigh matrix $a\ M_2 + b\ K_2$ in the discrete in space equation of motion. In the following, the strong form is employed to obtain the optimal conditions for minimizing the reflections at the interface as well as better describing the damping properties in the Rayleigh medium.

## 2.3 The problem of the wave propagation

### 2.3.1 Wave propagation in the Rayleigh medium

We study in this part the problem of the wave propagation in a damping medium characterized by the Rayleigh matrix into the discrete in space equation of motion. We assume that the medium is infinite and the wave propagates in the direction of $e_x$ (Figure 3).

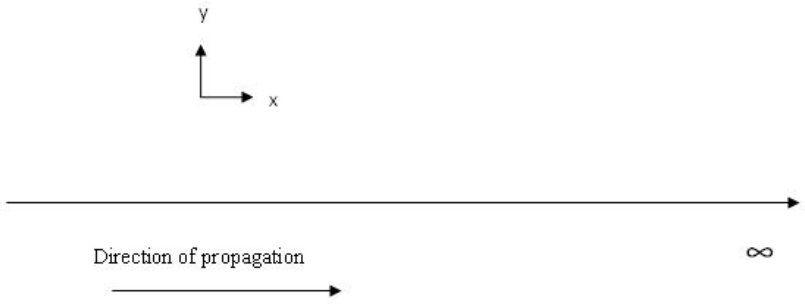


Figure 3: the problem of the wave propagation

Since the problem is 1D, the displacement can be put in the form: $u_2(x,t) = \widetilde{u}_2(x,t)\, e_x$ for P-waves or $u_2(x,t) = \widetilde{u}_2(x,t)\, e_z$ for S-waves.

The equation in the strong form Eq. (8) can be simplified as:

$$\rho_2\, \partial_t^2 \widetilde{u}_2 + a\, \rho_2\, \partial_t \widetilde{u}_2 = (\lambda_2 + 2\mu_2)\, \partial_x^2 \widetilde{u}_2 + b\, (\lambda_2 + 2\mu_2)\, \partial_x^2 \partial_t \widetilde{u}_2 \quad P - waves \tag{20}$$

$$\rho_2\, \partial_t^2 \widetilde{u}_2 + a\, \rho_2\, \partial_t \widetilde{u}_2 = \mu_2\, \partial_x^2 \widetilde{u}_2 + b\, \mu_2\, \partial_x^2 \partial_t \widetilde{u}_2 \quad S - waves \tag{21}$$

We consider an harmonic solution for the above equations in the following form:

$$\widetilde{u}_2(x,t) = T\ \exp(i(\omega_0\, t - k\, x)) \tag{22}$$

with $k$ is the complex wave number such as: $Re(k) \geq 0$.

By introducing this solution into the previous equations, we obtain the following wave number:

$$k^2 = (\frac{\omega_0}{V_2})^2 \frac{1 - a\, b - i(\frac{a}{\omega_0} + b\, \omega_0)}{1 + b^2\, \omega_0^2} \tag{23}$$

with the phase velocity $V_2$ equal to $\sqrt{\frac{\lambda_2 + 2\mu_2}{\rho_2}}$ for P-waves or $\sqrt{\frac{\mu_2}{\rho_2}}$ for S-waves.

We remark that the expression of $k$ is a complex number which depends on two parameters $a$ and $b$. It is convenient to choose them as:

$$\frac{a}{\omega_0} = b\, \omega_0 = \xi \tag{24}$$

$\xi$ being called the damping ratio.

We get:

$$\widetilde{u}_2(x,t) = T\ \exp(\frac{-\omega_0\,\xi\,x}{V_2\,\sqrt{1+\xi^2}})\ \exp(i(\omega_0\,t - \frac{\omega_0\,x}{V_2\,\sqrt{1+\xi^2}})) \tag{25}$$

Some interesting remarks can be done:

1. In order to have a logarithmic decrement of $\delta = \ln(\frac{|\widetilde{u}_2|(x)}{|\widetilde{u}_2|(x+\triangle x)})$, $\forall x$, the wave must travel a distance $\triangle x$ given by:
$$\triangle x = \frac{V_2}{\omega_0}\,\frac{\delta\,\sqrt{1+\xi^2}}{\xi} \tag{26}$$
We choose the largest value of $V_2$ (corresponding to the P-waves).
2. The phase velocity increases and becomes equal to $\sqrt{1+\xi^2}\,V_2$.

Next, we deal with non harmonic waves, by focusing on P-waves (the same results can be deduced for shear waves). Let us introduced $\widetilde{u}_2(x,t)$ the strong solution of the following problem:

$$\rho_2\,\partial_t^2\widetilde{u}_2 + a\,\rho_2\,\partial_t\widetilde{u}_2 = (\lambda_2+2\mu_2)\,\partial_x^2\widetilde{u}_2 + b\,(\lambda_2+2\mu_2)\,\partial_x^2\partial_t\widetilde{u}_2 \quad (x,\ t) \in ]0,+\infty[\times\mathbb{R} \tag{27}$$

with the boundary conditions :

$$\widetilde{u}_2(x=0,t) = f(t) \quad \forall t\ \in\ [0,+\infty[ \tag{28}$$

$$\widetilde{u}_2(x=0,t) = 0 \quad \forall t\ \in\ ]-\infty,0[ \tag{29}$$

and the initial conditions:

$$\widetilde{u}_2(x,\ t=0) = 0 \quad \forall x\ \in ]0,+\infty[ \tag{30}$$

$$\partial_t\widetilde{u}_2(x,\ t=0) = 0 \quad \forall x\ \in ]0,+\infty[ \tag{31}$$

here $f$ is a continuous map which satisfies the following conditions:

1. $f$ is integrable on $\mathbb{R}$
2. the Fourier transform of $f$ is integrable

The same expressions of $a$ , $b$ in Eq. (24) is adopted and we denote $\omega_0$ as the dominant angular frequency. By applying the Fourier transform for Eq. (27), it can be shown that the solution is given by:

$$\widetilde{u}_2(x,t) = \frac{1}{2\pi}\int\limits_{\mathbb{R}}\ \hat{f}(\omega)\ \exp(i(\omega\,t - k(\omega)\,x))\,d\omega \tag{32}$$

with the complex wave number defined by:

$$k(\omega) = \frac{\omega}{V_{p2}}\ \sqrt{\frac{1-\xi^2-i\xi(\frac{\omega_0}{\omega}+\frac{\omega}{\omega_0})}{1+\xi^2\,\frac{\omega^2}{\omega_0^2}}} \tag{33}$$

Here $\hat{f}$ is the Fourier transform of $f$ , $V_{p2}$ is equal to $\sqrt{\frac{\lambda_2+2\,\mu_2}{\rho_2}}$.

Now we are able, thanks to Eq. (32), to predict the behavior of the wave traveling through the Rayleigh medium. The problem of the spurious reflections at the interface will be discussed in the next section.

### 2.3.2 1D wave propagation from an elastic medium to a Rayleigh medium

Let us consider a elastic linear medium $\Omega_1$ and a Rayleigh medium $\Omega_2$ (section 2.1). We assume there is an harmonic wave (P-wave or S wave), which propagates from $\Omega_1$ toward $\Omega_2$ as shown in Figure 4.

The wave propagation problem is 1D and the main purpose is to quantify the spurious waves created at the interface.

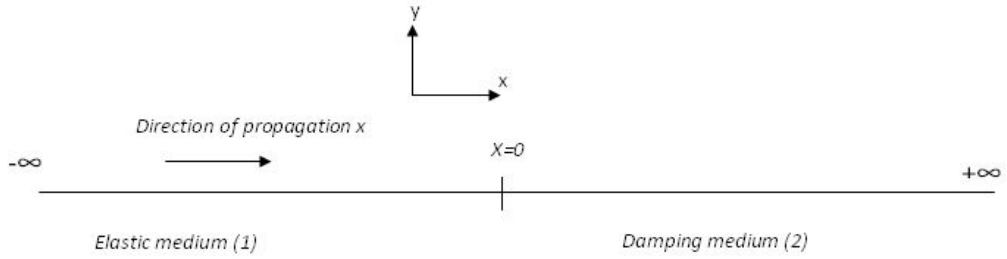


Figure 4: Wave propagation in two mediums separated by an interface $X = 0$

Let us called $\widetilde{u}_1$ is the incident wave, $\widetilde{u}_2$ the transmitted wave and $\widetilde{u}_R$ the reflected wave. Using the same values of the parameters $a$ and $b$, we write:

$$\widetilde{u}_1(x,t) = A\ \exp(i\omega_0\,(t - \frac{x}{V_1})) \tag{34}$$

$$\widetilde{u}_2(x,t) = T\ \exp(\frac{-\omega_0\,\zeta\,x}{V_2\,\sqrt{1+\zeta^2}})\ \exp(i(\omega_0\,t - \frac{\omega_0\,x}{V_2\,\sqrt{1+\zeta^2}})) \tag{35}$$

$$\widetilde{u}_R(x,t) = R\ \exp(i\omega_0\,(t + \frac{x}{V_1})) \tag{36}$$

where $V_i\ \{i = 1, 2\}$ is the phase velocity and is equal to : $\sqrt{\frac{\lambda_i+2\mu_i}{\rho_i}}$ for P-waves and $\sqrt{\frac{\mu_i}{\rho_i}}$ for S-waves.

From the conditions (section 2.1) at the interface (continuity of displacements and equilibrium of stresses), we have :

$$\widetilde{u}_2(x=0,t) = \widetilde{u}_1(x=0,t) + \widetilde{u}_R(x=0,t) \tag{37}$$

$$\kappa_2\,\partial_x\widetilde{u}_2(x=0,t) = \kappa_1\,(\partial_x\widetilde{u}_1 + \partial_x\widetilde{u}_R)\,(x=0,t) \tag{38}$$

with $\kappa_i\ \{i = 1, 2\}$ being equal to $\lambda_i + 2\mu_i$ for P-waves or $2\mu_i$ for S-waves.

We focus on the reflected waves generated at the interface. The reflection coefficient is given by:

$$\frac{R}{A} = \frac{1 - \gamma \sqrt{1 + \xi^2}}{1 + \gamma \sqrt{1 + \xi^2}} \tag{39}$$

with the parameter $\gamma$ defined by: $\gamma = \frac{\rho_2 V_2}{\rho_1 V_1}$

Now, we can give a condition under which the reflected P-waves and S-waves vanish as follows:

$$\gamma = \frac{1}{\sqrt{1 + \xi^2}} \tag{40}$$

For two subdomains, by choosing $\rho_1 = \rho_2$, the zero interface reflection coefficient condition writes as:

$$\begin{cases} \lambda_2 = \frac{\lambda_1}{1+\xi^2} & \mu_2 = \frac{\mu_1}{1+\xi^2} \\ E_2 = \frac{E_1}{1+\xi^2} & \nu_2 = \nu_1 \end{cases} \tag{41}$$

The results given by Eq. (41) show the relationships between the Young's modulus and Poisson's ratio for each material composing the subdomains. These results have been proved for harmonic waves and can be also used, as an approximation, for waves which have a dominant frequency.

In the following, non harmonic waves are considered. The incident wave is denoted $\widetilde{u}_1(x,t)$, satisfying $\widetilde{u}_1(x=0,t) = f(t)$ where $f$ is the same function defined in (section 2.3.1.). We can write $\widetilde{u}_1(x,t)$ as:

$$\widetilde{u}_1(x,t) = \frac{1}{2\pi} \int_{\mathbb{R}} \hat{f}(\omega)\ \exp(i(\omega\, t - \frac{\omega}{V_{1p}}\, x)) \tag{42}$$

Let introduce $\widetilde{u}_2(x,t)$ the transmitted wave and $\widetilde{u}_R$ the reflected wave. Taking into account the conditions at the interface (section 2.1), we can prove that $\widetilde{u}_2(x,t)$ and $\widetilde{u}_R(x,t)$ have the following expressions:

$$\widetilde{u}_R(x,t) = \frac{1}{2\pi} \int_{\mathbb{R}} \frac{1 - \gamma \sqrt{1 + \zeta^2 - i\,\zeta\,(\frac{\omega_0}{\omega} - \frac{\omega}{\omega_0})}}{1 + \gamma \sqrt{1 + \zeta^2 - i\,\zeta\,(\frac{\omega_0}{\omega} - \frac{\omega}{\omega_0})}}\, \hat{f}(\omega)\ \exp(i(\omega\, t + \frac{\omega}{V_1}\, x))\, d\omega \tag{43}$$

$$\widetilde{u}_2(x,t) = \frac{1}{2\pi} \int_{\mathbb{R}} \frac{2}{1 + \gamma \sqrt{1 + \zeta^2 - i\,\zeta\,(\frac{\omega_0}{\omega} - \frac{\omega}{\omega_0})}}\, \hat{f}(\omega)\ \exp(i(\omega\, t - k(\omega)\, x))\, d\omega \tag{44}$$

The above expressions will be employed as reference results in the section devoted to numerical examples by using Discrete Fourier Transforms available in Matlab software. Derived reference results will be compared with numerical solutions obtained with finite element method along with a time integration scheme.

## 3 Numerical examples

Finite element method is employed for checking previous theoretical observations. We start by choosing a Ricker wave [14] $R$ as an incident wave defined by :

$$R(t,\, t_p,\, t_s) = A\,(2\,\pi^2\,\frac{(t-t_s)^2}{t_p^2} -\, 1)\,\exp(-\pi^2\frac{(t-t_s)^2}{t_p^2}) \tag{45}$$

We observe that the Ricker wave depends on three parameters $t_p$, $t_s$ and $A$ chosen equal to $3,\ 3,\ 1$ respectively. The displacements are imposed at a given point according to the Ricker function, characterized by one dominant frequency equal to $\frac{1}{t_p}$ (Figure 5).

The first example deals with a 1D wave propagation in the damping Rayleigh medium. Numerical solution using an implicit time integration is validated against the reference results obtained by Discrete Fourier Transform and Discrete Inverse Fourier Transform using Matlab according to Eq. (32). Then, it will be shown that the condition in Eq. (40) minimizes the reflected waves by computing wave propagation from an elastic medium towards a damping Rayleigh medium separated by an interface. Finally, the 2D propagation problem from Lamb is dealt with the explicit/implicit multi-time step co-computations. An external coupling software is used, coupling the explicit FE code Europlexus with fine time step for the domain of interest with implicit FE code Cast3m with macro time step for the Rayleigh damping layer.

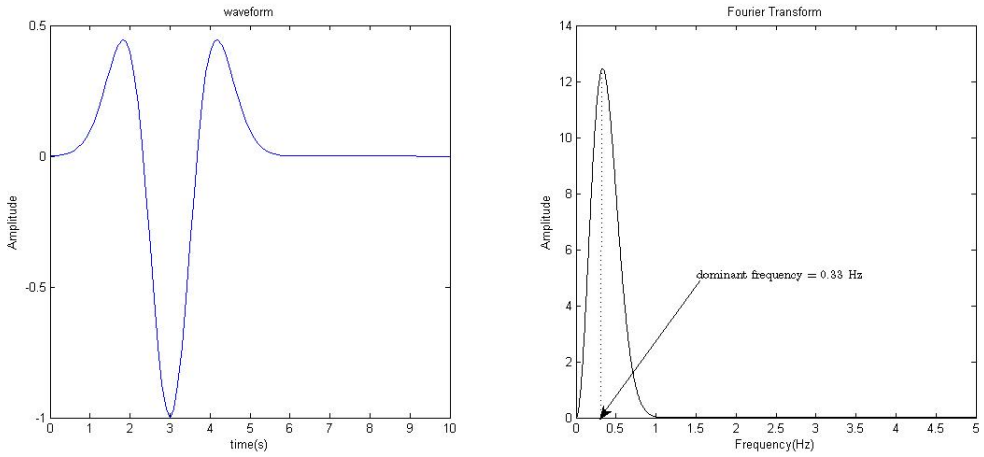


Figure 5: Input displacement (Ricker wavelet) and Amplitude of its Fourier transform

### 3.1 1D wave propagation in the Rayleigh damping material

In this part, we consider a problem of P-wave.The solution given by the finite element method will be computed using Castem software[13]. The semi-infinite layer is modeled using a bounded domain shown in Figure 6. A uniform finite element mesh of four-node rectangular elements, each one having the size of $\frac{\lambda}{50}$, is used to discretize the problem. From the displacement imposed point $x = 0$, the length of the mesh extends to a distance of $5\lambda$ ($\lambda$ being the wave length of the Ricker wave). The mesh is chosen to be very large so as to avoid the interference between the incident wave and the reflected waves, which propagates back toward the displacement imposed point.

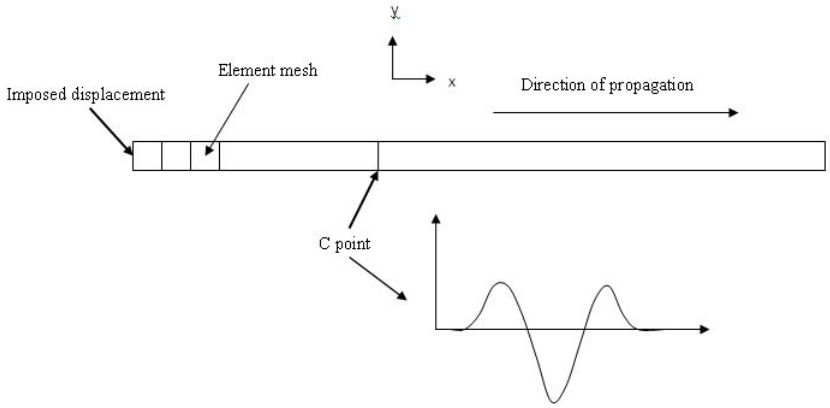


Figure 6: Homogeneneous damping layer of length $5\lambda$

Finally, the displacement is imposed in the direction of $x$ and we choose a point $P$ at $x = 100\ m = 0.4\lambda$ to compare the time-history response predicted by the finite element code and the reference solution according to Eq. (32). In finite element code, an implicit time integration scheme has been adopted. Here, it has to be reminded that only one domain is considered.

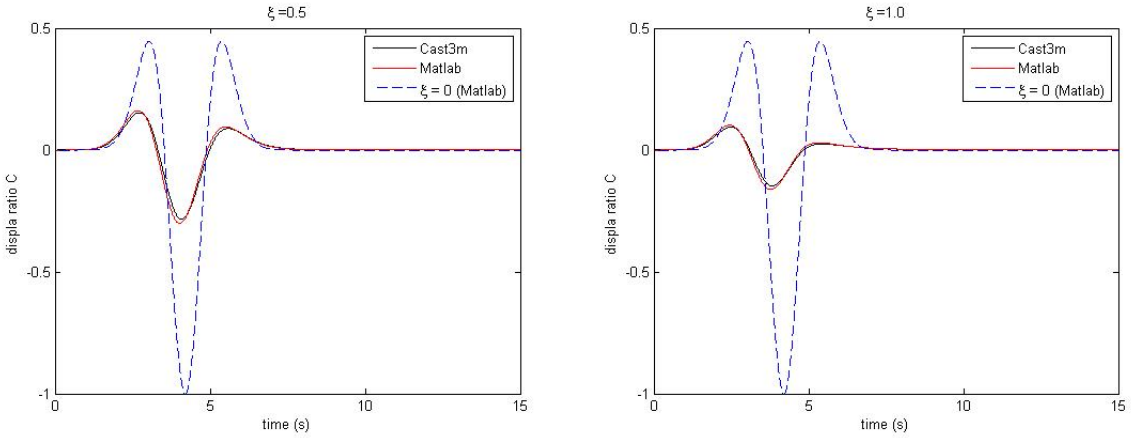


Figure 7: displacement in the point C, $\omega_0 = \frac{2\pi}{t_p} = 2.09$ , $\xi = 0.5$ (left) , $\xi = 1$ (right)

Figure 7 presents the displacement ratio $(\frac{\widetilde{u}_2(x,t)}{A})$ computed at the point C using Cast3m and Matlab (reference results) against the solution without damping ($\xi = 0$), also computed using Matlab. The results obtained from Cast3m are very close to the reference results. From Figure 7, it can be verified that the numerical phase velocity in the Rayleigh damping domain is greater than the phase velocity in an undamped domain.

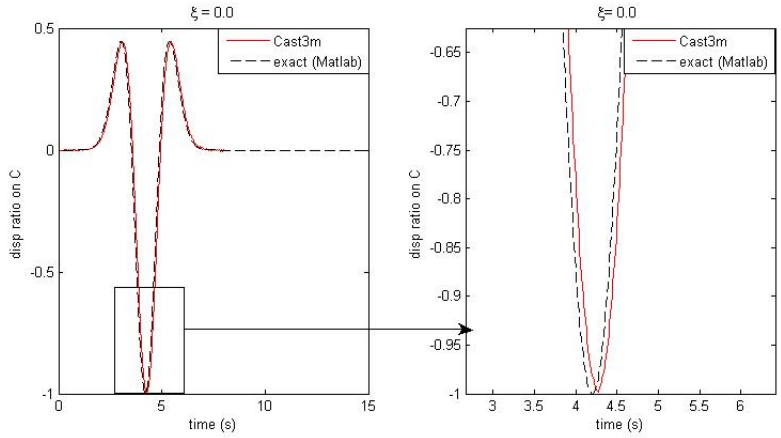


Figure 8: The difference between the numerical phase velocity and the exact phase velocity

From Figure 9, we observe that the numerical solution is more damped than the reference one. This remark can be justified by the following observations . Assuming a quasi harmonic wave, that is with a dominant frequency, it can be seen in Figure 8 that the numerical phase velocity $V_{p2}^{num}$ without viscous damping is lower than the reference velocity $V_{p2}^{real}$ without viscous damping. So, when considering Rayleigh damping medium with $\xi$ the damping ratio, the following relationship between the logarithmic decrements can be written:

$$\delta^{real} = \frac{d\,\xi\,\omega_0}{V_{p2}^{real}\sqrt{1+\xi^2}} \leq \frac{d\,\xi\,\omega_0}{V_{p2}^{num}\sqrt{1+\xi^2}} = \delta^{num} \tag{46}$$

where $d$ is a constant distance. It means that the numerical logarithmic decrement $\delta^{num}$ is greater than the reference logarithmic decrement $\delta^{real}$ underlined in Figure 9, where the displacemnt peaks of Figure 7 have been zoomed.

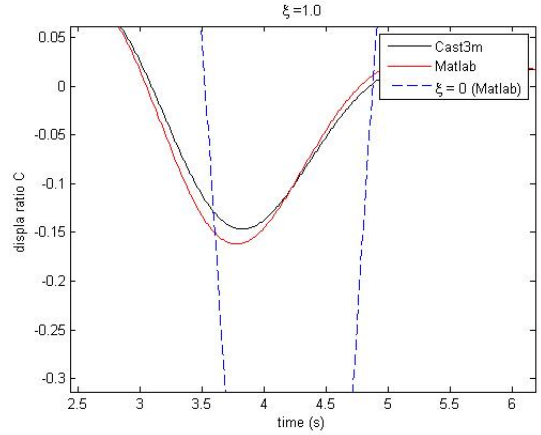


Figure 9: Zoom on the displacement computed on C for the case $\xi = 1$

### 3.2 1D wave propagation from an elastic medium towards the Rayleigh damping medium separated by an interface

In order to validate the theoretical results obtained in the section 2.3.2, we start by considering the problem illustrated in Figure 4. The characteristics of the two material are summarized in the following table :

| | Domain 1 (Hooke material) | Domain 2 (Damping material) |
|---|---|---|
| Young's modulus ( $MPa$ ) | 10 | Variable |
| Poisson's ratio | 0.24 | 0.24 |
| Element size | $\frac{\lambda}{50}$ | $\frac{\lambda}{50}$ |
| Type of element | rectangular (linear) | rectangular (linear) |
| Mesh length | $5\lambda$ | $5\lambda$ |
| Mass density ( $Kg/m^3$) | 1700 | 1700 |

Table 1: Characteristics of materials

We impose the displacement at the point $x = -5\lambda$ according to the same Ricker wave as previously. Then, we compute the displacement at the point $C$ located at $0.4\lambda$ from the imposed displacement point. Here we can observe that the point C is far enough from the interface $x = 0$ to avoid the interference between the reflected wave and the incident wave. The Young's modulus of the domain 2, as given in Table 1, is dependent on the damping ratio as: $\gamma = \frac{1}{\sqrt{1+\xi^2}}$. The Figure 10 displays the comparison of results between the FE method using Cast3m with an implicit time integration scheme and the reference results using Matlab according to Eq. (43) for several values of $\xi$.

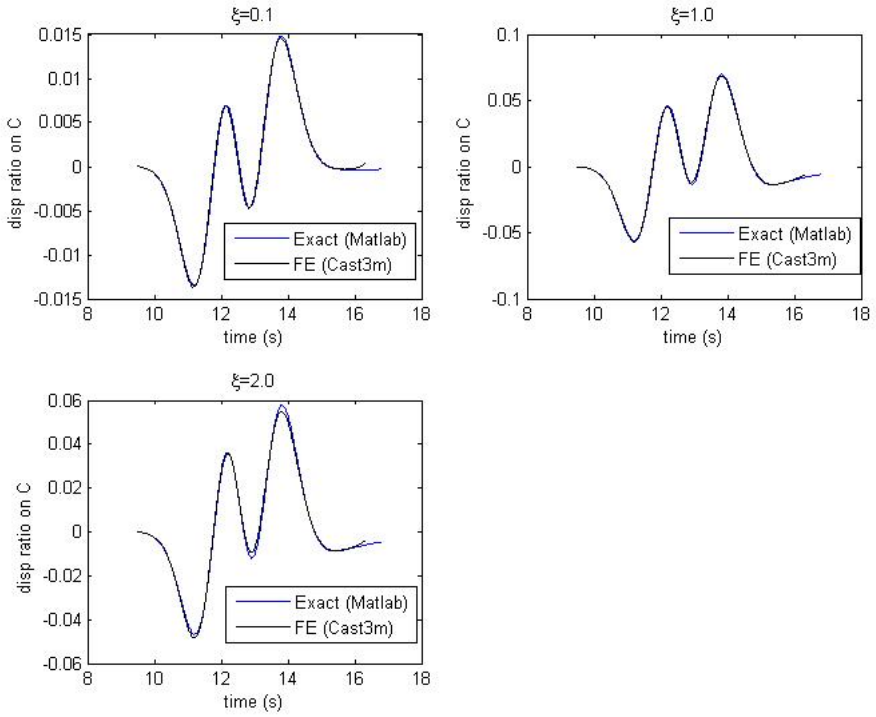


Figure 10: Refelected wave computed on point C, $\omega_0 = \frac{2\pi}{t_p} = 2.09$

From the Figure 10, we remark that both curves (numerical and reference results) are in very good agreement for different values of $\xi$. In the first case $\xi = 0.1$, the wave is reflected with a ratio of $1.5\%$ which is much lesser than the other cases: $5,5\%$ for $\xi = 1$ and $6\%$ for $\xi = 2$.

We want to check the condition about the Young modulus $E_2$ of the damping layer so as to minimize the reflected waves at the interface. For this purpose, we realize a simple test

using Cast3m in which we vary the value of $E_2$ within a range, $\xi$ remaining constant as well as the parameters $\nu_2$, $\rho_2$ equal to $\nu_1$, $\rho_1$ respectively. For each value of $\xi$, the value of $E_2$ which minimizes the reflections at the interface is determined. In Figure 11, the identified optimal value of $E_2$ is compared with the theoretical condition, that is: $\gamma(\xi) = \frac{1}{\sqrt{1+\xi^2}}$. It can be seen that the numerical identified curve matches very well the theoretical curve. It is important to note that the condition $\gamma(\xi) = \frac{1}{\sqrt{1+\xi^2}}$ for minimizing the reflected waves at the interface has been obtained for harmonic waves. From Figure 11, it can be concluded that this condition provides a good approximation for non harmonic waves such as the ricker wave as well.

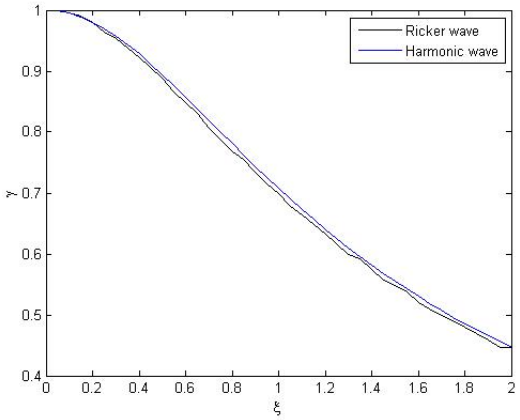


Figure 11: Values of $\gamma$ miminizing the amplitude of the reflected waves for the both waves ( theoretical curve with harmonic waves and numerical curve with a Ricker wavelet)

### 3.3 2D Lamb test using explicit/implicit multi-time step co-computations

The Lamb test consists in applying a concentrated load at the surface of a ground assumed to be infinite in the direction of both directions. A sensor is located at a distance $d = 10\,m$ from the load point for the purpose to recording the vertical and the horizontal displacements at this point (Figure 12). In 1904 Lamb [11] analytically calculated the displacements at a given point of the surface by assuming an isotropic linear elastic behavior of the soil. The theoretical solution shows the complexity of the problem since there are many types of waves traveling through the soil (P and S-waves, Rayleigh waves, $etc$). In this part, we will compute the numerical solution using the explicit/implicit multi time step GC method. Two FE codes are involved into the tho co-computations: Europlexus code based on a explicit time integration scheme for the domain of interest and implicit Cast3m code for the damping layers by adopting a large time step for reducing the time computation. The time step ratio between the macro time step (implicit FE code) and the micro time step (explicit FE code) is set to 50.

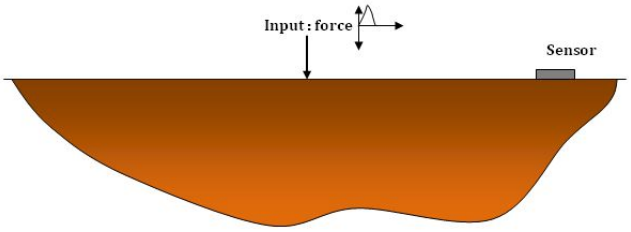


Figure 12: Lamb test

In order to use the GC method we have to divide the problem into 2 subdomains (Figure 13): subdomain 1 models the soil assumed to be linear elastic with $\rho_1 = 1700\ kg/m^3$, $E_1 = 10MPa$ and $\nu_1 = 0.24$ and the subdomain 2 models the Rayleigh damping medium with $\rho_2 = 1700\ kg/m^3$ and $\nu_2 = 0.24$ . The Rayleigh matrix has the following parameters: $\xi = 0.1$ and $\omega_0 = \frac{2\pi}{t_p}$ according to Eq. (24). The soil is modeled by a rectangle surrounded by the damping layer of thickness $e$. A concentrate load is applied at the middle of the surface, defined by a Ricker wavelet with the parameters: $A = 1MN\ t_p = 3\ t_s = 3$. Figure 14 presents the meshes used for this simulation, the soil is modeled by Europlexus code (the symmetry is taken into account) using rectangular elements with size of $\frac{\lambda}{50}$ and the Rayleigh damping medium is modeled by Cast3m code using the same size of elements as in the subdomain 1.

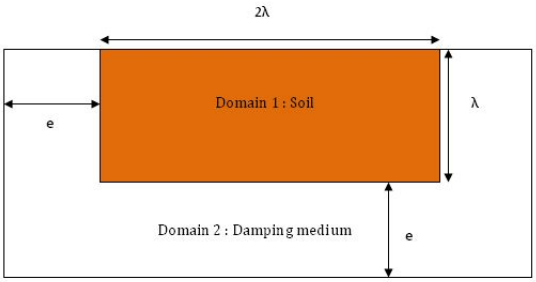


Figure 13: The shapes of the domains

The damping layer is defined by a logarithmic decrement target $\delta = \ln(10)$ leading to a thickness of $e = 914\ m = 3.6\ \lambda$ by using the condition in Eq. (26). Furthermore, we choose a point C close to the load point with a distance equal to $10\ m$ at which the horizontal and vertical displacements will be plotted.

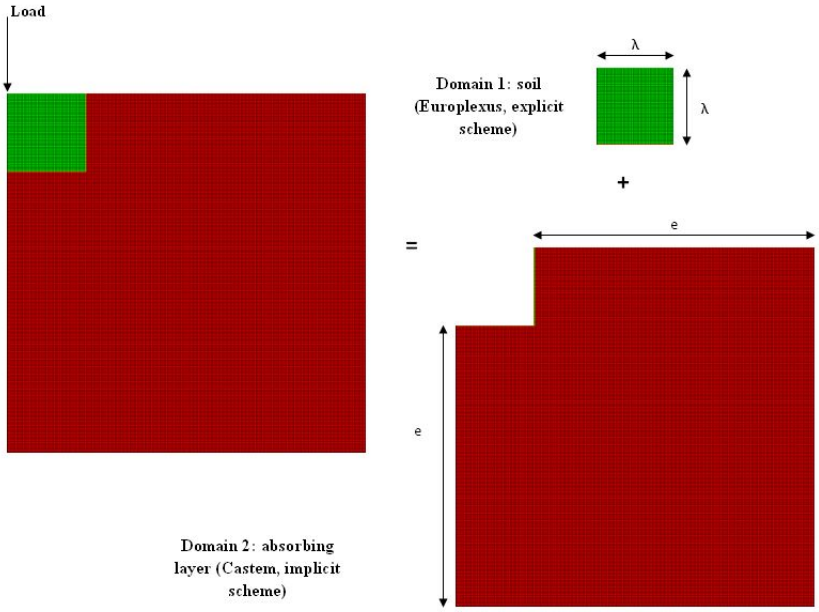


Figure 14: The mesh used for the GC method : domain 1 (soil) modeled by Europlexus and the domain 2 (absorbing medium) modeled by Castem

In Figure 15, the results computed at the point C using the Rayleigh damping layer are compared with Lamb analytical solutions using Matlab. An additional numerical solution is provided by using classical viscous dampers at the absorbing boundaries available in Cast3m code. An implicit time integration is adopted with this method, without considering subdomain decomposition. We remark that the results obtained by the absorbing boundary method are not accurate enough with respect to the exact solution (Matlab). It is due to artificial reflections at the interface. It has to be highlighted that our explicit/implicit multi-time step strategy with Rayleigh damping layers provides numerical results in very good agreement with respect to the reference solution. Consequently, it has been shown: 1- the approximate condition in Eq. (40) enables to efficiently minimize the reflected waves at the interface although this condition is strictly valid for harmonic waves with a normal incidence. 2- the multi-time step GC method is successively employed, enabling to gain computational performance by taking large time step in the Rayleigh damping layer. It is important to note that the GC method generates some spurious damping at the interface as soon as different time steps are employed for subdomains as proven in [8]. Thus, it can be concluded that this effect is not important in our simulation.

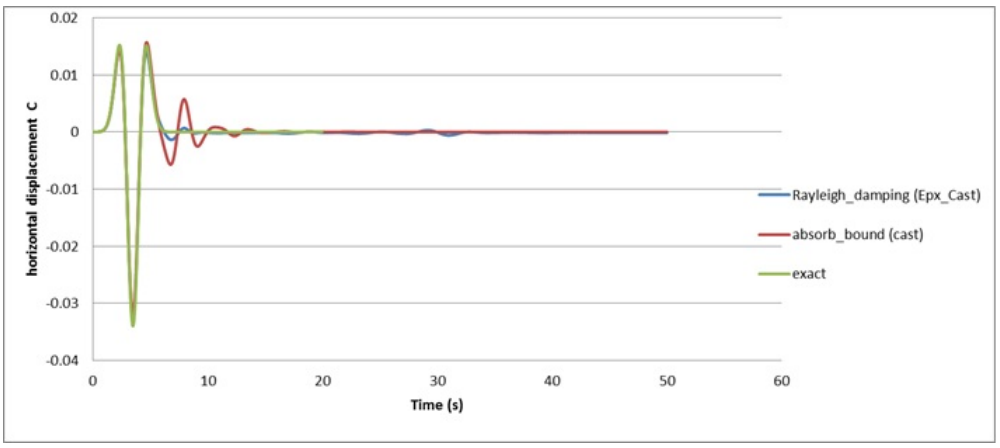


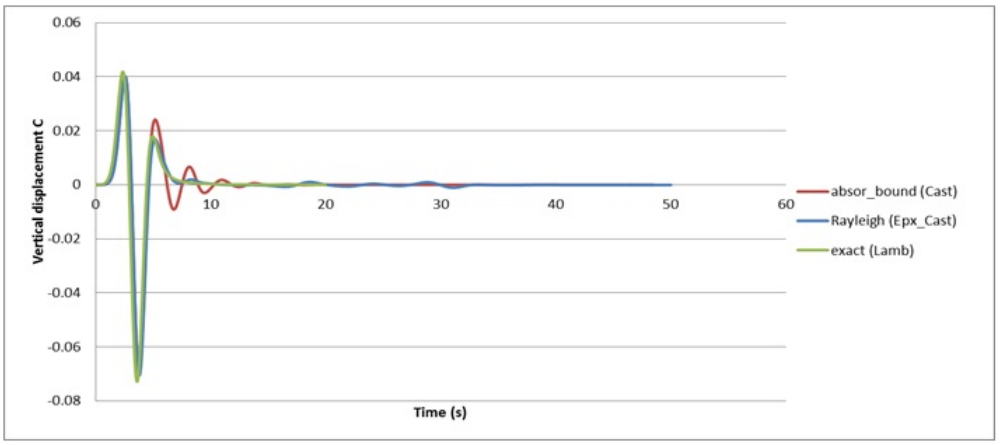


Figure 15: Horizontal and vertical displacements plotted on C obtained by Rayleigh damping (blue curve) , Absorbing boundaries (red curve) and the exact solution ( Lamb) (green curve)

## 4 Conclusion

In this paper, a strong form for wave propagation in a damping Rayleigh medium is given. It has been shown that the proposed strong form exactly corresponds to the introduction of the Rayleigh matrix into the discretized equation of motion by the finite element method. This strong from is employed to derive optimal conditions for minimizing the reflected waves appearing at the interface between two media with different damping ratios in the case of harmonic waves. Analytical results using discrete Fourier transform in Matlab and numerical results using finite element code demonstrate the relevance of this optimal condition for a non harmonic Ricker wave. Explicit/implicit multi time step co-computations involving two FE codes (explicit for the domain of interest and implicit for the Rayleigh damping layers) have been successfully carried out. The proposed approach turns out to be very accurate in comparison to the reference results and the ability to choose a large time step in the Rayleigh damping layer enables to improve the computation performance of the proposed numerical strategy accounting for unbounded medium.

## REFERENCES

[1] J.P. Wolf, *Dynamic Soil–Structure Interaction*, Prentice-Hall, Englewood Cliffs, NJ, 1985.

[2] Basu U, Chopra AK, Perfectly matched layers for time-harmonic elastodynamics of unbounded domains: theory and finite-element implementation. *Int J Numer Methods Eng*, 192 ,1337-1375, 2003.

[3] Engquist B, Majda A, Absorbing boundary conditions for the numerical simulation of waves. *Mathematics of Computation*, 31, 629-65, 1977.

[4] Bettess P, Infinite elements. *International Journal for Numerical methods in Engineering*, 11, 53-64, 1977.

[5] Semblat JF,Gandomzadeh A, Lenti L,A simple numerical absorbing layer method in elastodynamics. *C. R. Mecanique*, 338, 24-32, 2010.

[6] Clough RW, Penzien J, *Dynamics of stuctures*, McGraw-Hill Compagnies, 634 p,1975.

[7] Semblat JF, Rheological interpretation of Rayleigh damping. *Journal of Sound and Vibration*, 206, 741-744, 1997.

[8] Gravouil A, Une mthode multi-chelle espace-temps pour le calcul de la dynamique transitoire des structures, PhD Thesis, ENS Cachan, France, 2000.

[9] Hughes TJR, *The Finite Element Method: Linear Static and Dynamic Finite Element Analysis*, Prentice-Hall, Englewood Cliffs, NJ, 1987.

[10] Brun M, Batti B, Limam A, Combescure A, Implicit/explicit multi-time step co-computations for predicting reinforced concrete structure response under earthquake loading. *Soil Dynamics and Earthquakes Engineering*, 33, 19-37, 2012.

[11] Lamb H, On the propagation of tremors over the surface of an elastic solid. *Proceedings of the Royal Society of London*, 72, 128-130, 1903.

[12] Europlexus , *User's manual*, 2006 (www.europlexus.jrc.ec.europa.eu).

[13] Cast3m, *Presentation et utilisation de Cast3m*, 2011(www.cast3m.cea.fr).

[14] Semblat JF, Pecker A, *Waves and vibrations in soils*, IUSS Press, 499 p, 2009.

[15] Meza-Fajarado KC, Papageorgiou AS, A nonconvolutional, Split-Field, Perfectly matched layer for wave propagation in isotropic and anisotropic elastic media: stability analysis. *Bulletin of the Seismological Society of America*, 98, 1811-1836, 2008.

[16] Allaire G, *Analyse numrique et optimisation : Une introduction la modelisation mathmatique et a la simulation numerique*, Ecole Polytechnique, 459 p, 2005